INVITED FEATURE PAPER

Enhanced water oxidation efficiency of hematite thin films by oxygen-deficient atmosphere

André L.M. Freitas, Waldemir M. Carvalho Jr., and Flavio L. Souza[a)]
Laboratory of Alternative Energy and Nanomaterial (LEAN), Centro de Ciências Naturais e Humanas (CCNH), Universidade Federal do ABC (UFABC), Santo André, São Paulo 09210-580, Brazil

(Received 7 July 2015; accepted 26 October 2015)

This work describes the effects of different atmospheres used during the thermal treatment of hematite films synthesized on transparent conductive substrates of fluorine-doped tin oxide by a newly reported wet chemical route assisted by microwave. The as-synthesized films were subjected to additional thermal treatment at 750 °C for 30 min in different gas flux (air, O_2, and N_2) to obtain a desirable phase and surface activation. A series of techniques were used to elucidate effects of each atmosphere used during the thermal treatment. The morphology of the films, as analyzed by top-view and cross-sectional scanning electron microscopy images, showed no significant changes and was composed of rods homogeneously distributed over the substrate, which covered the immersed area with a thickness between 98 and 100 nm. The photoelectrochemical response of the N_2-hematite films was found to be 80 and 50% more efficient at 1.23 V_{RHE} (reversible hydrogen electrode) than those of films produced in air and an O_2 atmosphere. The photocurrent enhancement achieved by treatment in an oxygen-deficient atmosphere was attributed to the improvement of hematite catalytic activity, which produced a hematite–electrolyte interface favorable for water oxidation. Since an increase in the donor density by one order of magnitude was found for the N_2-hematite films, a reduction of charge transfer resistance was expected in these films. However, the Nyquist plot analysis showed that the O_2-hematite film had a lower charge transfer resistance. As a result, it is impossible to relate the photocurrent enhancement observed in N_2-hematite film to electronic changes or vacancy formation, as previously reported in the literature. Indeed, by performing photoelectrochemical measurements in the presence of hole scavengers, it became clear that the major improvement caused by the oxygen-deficient atmosphere was in the catalytic activity efficiency of the hematite films for water oxidation. It was found that the oxygen-deficient atmosphere could improve the overall photoelectrochemical performance of the hematite by acting as a hole scavengers. This finding contrasts with a previous report, in which the use of an oxygen-deficient atmosphere during the phase transformation from akaganeite to hematite was found to enhance the photocurrent density by inducing an increased donor density caused by the formation of vacancies [Y. Ling et al., *Angew. Chem., Int. Ed.* **51**, 4074 (2012)].

I. INTRODUCTION

Iron oxide (hematite) is considered to be a promising material with good properties for application in photoelectrochemical cell (PEC), which uses sunlight to split water into molecular hydrogen and oxygen. Hematite fulfills most of the important requirements for materials in PEC applications, such as high natural abundance, good electrochemical stability, and possessing a band gap favorable for the absorption of sunlight, which is mostly concentrated in the visible range of the electromagnetic spectrum. However, the very low sunlight conversion efficiency achieved by hematite has limited its application in commercial devices. This low conversion efficiency is the result of specific limitations, such as the short lifetime of minority charges (holes) and the small optical absorption coefficient of hematite. In the last decades, much research has been dedicated to the study of the properties of hematite to overcome these limitations.[1–12] However, the properties of the material still require better understanding in order for researchers to achieve progress in the use of hematite as a photoanode. Bard and Hardee reported the first uses of hematite films in PECs, using hematite synthesized via chemical vapor deposition.[13,14] Since Graetzel and co-workers[15] introduced the concept of downsizing a material to the nanoscale to improve the properties of the bulk material,

Contributing Editor: Edson Roberto Leite
[a)]Address all correspondence to this author.
e-mail: fleandro.ufabc@gmail.com or flavio.souza@pq.cnpq.br
This paper has been selected as an Invited Feature Paper.
DOI: 10.1557/jmr.2015.353

 © Materials Research Society 2015

https://doi.org/10.1557/jmr.2015.353 Published online by Cambridge University Press

nanoscience has provided a new perspective. Nanomaterials have become essential for the development of several synthetic routes[16–24] to fabricate efficient nanostructured hematite photoanodes for applications in PECs. Recently, aqueous chemical routes under hydrothermal conditions and colloidal approaches have been considered to be very promising methods for the synthesis of films on a large variety of substrate materials, with relatively low costs and easy scaling of the processes.[25–33] After many reports had demonstrated the generation of interesting hematite morphologies in the nanoscale by means of several physical and chemical techniques, including the chemical approaches mentioned above, several strategies were used to improve the optical absorption coefficient and poor electronic conductivity of nanoscale hematite.[34] Among these strategies, the incorporation of dopants[35–38] and the deposition of different materials as under- or over-layers[39] have been observed to be the most effective to enhance the efficiency of hematite as a photoanode material. In addition, the careful control of the thermal treatment conditions, such as the temperature and atmosphere, seems to be crucial to the good performance of both pure and modified hematite electrodes for water oxidation under irradiation by sunlight.[40–43]

Ling and co-authors[44] reported the influence of thermal treatment in an oxygen-deficient atmosphere on the performance of hematite. They found that the presence of oxygen vacancies in the hematite structure significantly affected the overall photoelectrochemical response of the material. Li and coworkers also investigated the effect of an oxygen-deficient atmosphere on the decomposition of akaganeite to the desirable hematite phase; they attributed the enhancement of the photocurrent to an increased donor density resulting from the formation of oxygen vacancies.[44] However, after several years of investigation to elucidate the mechanism controlling the changes caused by oxygen-deficient atmospheres on hematite films, a consensus has not yet been reached. Recently, in revisiting the investigation of the effects of an oxygen-deficient atmosphere on the properties of hematite film, Li and coworkers conducted a systematic and detailed kinetic analysis to elucidate a complete mechanistic model of the operation of oxygen-deficient hematite electrodes.[45] They showed that the balance between the enhanced electrical properties and trap-mediated losses is responsible for the enhanced photoelectrochemical water splitting efficiency of hematite electrodes prepared by a wet chemical method and modified by the deposition of an Al_2O_3 overlayer.

In this context, we describe the single-step synthesis of akaganeite films by an aqueous precursor solution kept under hydrothermally assisted conditions using a commercial microwave oven. To obtain the desired hematite phase and activate the surface of the hematite film for water oxidation, an additional thermal treatment at 750 °C for 30 min was performed under different atmospheres of air, O_2, and N_2. Several techniques were used to fully characterize the role of the atmosphere on the overall performance of hematite films. The best improvement in the performance of hematite film was achieved by using an oxygen-deficient atmosphere, which increased the catalytic activity of the films for water oxidation. The results of this study contrast with those reported in the literature, in which the authors investigated the effect of an oxygen-deficient atmosphere on the phase transformation from iron oxyhydroxide to hematite and related the resulting improvement in the photocurrent exclusively to the increased donor density by vacancy formation.[44]

II. MATERIALS AND METHODS

Nanostructured iron oxide thin films were prepared from an aqueous solution assisted by microwave. The approach utilized the dissolution of ferric chloride ($FeCl_3 \cdot 6H_2O$, Vetec, Rio de Janeiro, Brazil; 97%) and sodium nitrate ($NaNO_3$, Vetec; 99%) in deionized water [resistivity (ρ) > 17 MΩ/cm] with a pH of 1.5 after adjustment with chloride acid (HCl, Nuclear, São Paulo, Brazil; 36.5–40%). Commercial transparent conductive glass substrates of fluorine-doped tin oxide (FTO, ρ = 10–15 Ω/cm) were cleaned and then immersed in a special bottle (capacity 30 mL) containing 15 mL of the precursor solution. The system comprising the bottle, solution, and substrate was subjected to hydrothermal conditions controlled by a commercial microwave (Monowave 300, Anton-Paar, Estiria, Austria) at a constant temperature of 100 °C for 2 h. Subsequently, the substrates and newly formed films were cleaned three times with deionized water to remove any residual salts from the precursor solution from the surface of the films. To obtain the desired crystalline phase the iron oxide thin films were submitted an additional thermal treatment. The temperature of thermal treatment at 750 °C/30 min was chosen based in a systematic investigation about the influence of the temperature and time of thermal treatments performed to obtain high-purity hematite phases, recently reported by our group.[46] To evaluate the influence of the atmospheric composition on the quality of the as-synthesized films, thermal treatments at 750 °C for 30 min were conducted under three different gas fluxes of air, O_2, or N_2 in a tube furnace (Lindberg/Blue M Mini-Mite TF55030; Thermo Fisher Scientific, Asheville, North Carolina).

The optical properties of the films were measured using a Varian Cary 50 spectrophotometer (Varian Inc., Santa Clara, California) in the range of 200–800 nm. The film morphologies were characterized by scanning electron microscopy (FEG-SEM, FEI Inspect F50; FEI Company, Hillsboro, Oregon) and atomic force microscopy (Agilent 5500 microscope; Agilent, Santa Clara, California) using an intermittent contact mode. The structural phases were determined by x-ray diffraction using Cu K_α radiation (XRD, D8 Focus, Bruker AXS; Bruker Corporation, Karlsruhe, Germany) in a 2θ range from 10 to 80°, with a step scan of 0.02° and 3 s/step.

https://doi.org/10.1557/jmr.2015.353 Published online by Cambridge University Press

Photoelectrochemical characterization was performed using linear sweep voltammetry (current density, J, versus E) under both dark and illuminated conditions. The light conditions were simulated using a 450 W Xe lamp (O_3-free) coupled with an AM 1.5 G filter. The light intensity was set to 100 mW/cm^2. In addition, the stability of the current within the films was analyzed by chronoamperometry (J versus time t). Electrochemical impedance spectroscopy (EIS) measurements were also obtained. The EIS data were analyzed by a Mott–Schottky plot of C^{-2} versus V_{RHE}, which allowed the determination of the charge carrier density (N_D) and the depletion layer width (W). For this purpose, a three-electrode Teflon electrochemical cell with a quartz window was coupled to a potentiostat/galvanostat (μAutolab III; Metrohm Autolab, Utrecht, The Netherlands) with a frequency response analyzer.

The incident photon-to-current conversion efficiency (IPCE) was measured as a function of the excitation wave length (λ) using a 300 W Xe lamp (O_3-free) coupled to a Cornerstone 260 monochromator (Oriel Quantum Efficiency Measurement Kit; Newport Corporation, Irvine, California). The IPCE (measured as a percentage) was calculated using the following equation:

$$\mathrm{IPCE} = (I(\lambda)1240/E(\lambda)\lambda)100 \quad , \qquad (1)$$

where $I(\lambda)$ is the photocurrent density (μA/cm^2) and $E(\lambda)$ is the irradiance (μW/cm^2).

III. RESULTS AND DISCUSSIONS

The precursor solution maintained at constant temperature (100 °C) for 2 h under hydrothermal conditions well-controlled by a commercial microwave resulted in an as-synthesized film covering the entire immersed area of the conductive glass substrate in the form of a thin yellow layer [Fig. 1(a), inset]. The yellow layer is composed of the akaganeite phase (iron oxyhydroxide, β-FeOOH) as illustrated in Fig. 1(a), in which the XRD peaks are indexed using the 34-1266 JCPDS card as a reference. To obtain the desired hematite phase (α-Fe_2O_3) for this study, the thin films were thermally treated at 750 °C for 30 min in a tube furnace under different atmospheres. As mentioned in the experimental section to the materials and method section, the as-synthesized film samples were thermally treated under an open atmosphere (henceforth referred to as Air–Fe_2O_3), a continuous flow of N_2 gas (N_2–Fe_2O_3), and a continuous flow of O_2 gas (O_2–Fe_2O_3), resulting in a transparent orange-red film, as exemplified in the inset picture of Fig. 1(b). To guarantee the reproducibility and quality of the present study, thin films were prepared in triplicate for each thermal treatment condition used to produce a total of 9 films. The structural transition arising from the thermal treatment was monitored by XRD.

Figure 1(b) exhibits the diffractograms of the orange-red thin films obtained after the additional thermal treatment under different atmospheres. All reflection peaks are readily indexed using the standard hematite powder diffraction data JCPDS catalog (33-0664) as reference, which confirms the formation of a pure hematite phase for all thermally treated thin films. As expected, peaks correlating to additional phases do not appear, except for the peaks corresponding to the transparent conductive material of the substrate, which are indexed as SnO_2 (cassiterite phase). Additionally, the XRD data permitted the estimation of the degree of film orientation F, using a relationship originally proposed by Lotgering's equation[47,48]:

$$F = P - P_0/1 - P_0 \quad , \qquad (2)$$

where $P = \sum I(h00)/I(hkl)$, I is the intensity of the diffraction peak obtained experimentally, and P_0 is the value of P calculated with standardized data from the JCPDS spectrum of a polycrystalline sample. Generally, higher degrees of orientation, indicated by larger values of F, relate to the preferred crystallographic orientations (O.P.) of the analyzed samples.

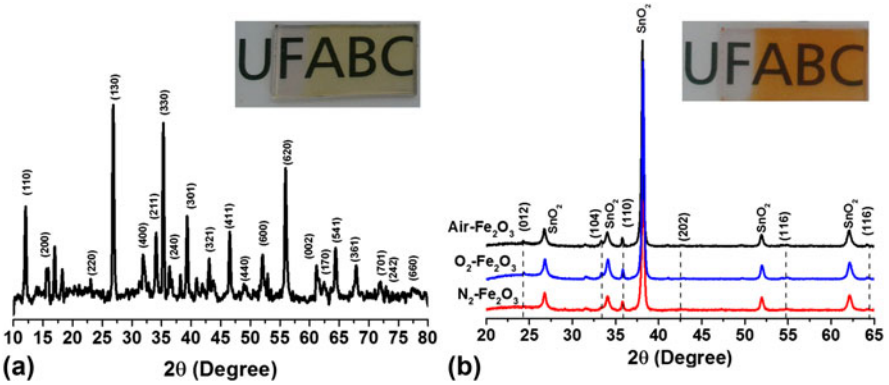


FIG. 1. XRD patterns of iron oxide films synthesized during 2 h microwave-assisted wet chemical reaction, with additional thermal treatment at 750 °C for 30 min in the different atmospheres of air, O_2, and N_2. (a) As-synthesized films and (b) thermally treated films. Inset photographs in (a) and (b) depict a film before and after the thermal treatment process, respectively.

https://doi.org/10.1557/jmr.2015.353 Published online by Cambridge University Press

According to the O.P. calculations, the thermally treated films exhibited a preferred growth direction growth in the (110) diffraction plane for all hematite samples. Furthermore, the orientation degree F increased from 0.273 in air to 0.305 with O_2 treatment. F increased further to 0.588 with N_2 treatment. It is generally accepted that good conductivity can be achieved in a hematite electrode by generating a nanostructured film with a diffraction peak from the hematite crystal oriented preferentially in a direction parallel to the substrate, which means that the basal plane of (001) is oriented perpendicular to the substrate. This strategy guarantees the more efficient charge collection of the hematite, consequently enhancing the conductivity of the film by up to four orders of magnitude.[11,12,18,21,44] As a consequence of this increased conductivity, this property of hematite as applied as a photoanode in PEC devices favors the charge transfer through the depletion layer. The charge injection to the back contact thus reduces the recombination rate and increases the efficiency of the cell.[16,49] The importance of crystal alignment and the improvement provided when the hematite crystals are well-aligned in the (110) plane have been discussed in detail in several reports.[21,32] The effect of the degree of orientation estimated from the XRD patterns will become more apparent during later discussion of the photoelectrochemical measurements of the films.

The morphologies of the films and the effects caused by thermal treatment under different atmospheres can be observed by the top-view and cross-sectional SEM images presented in Fig. 2. The top-view SEM images depict similar nanostructured morphologies composed of rods in all films with apparent porosity and homogenous distributions of rods over the substrate areas, independent of the atmosphere of the thermal treatments, [Figs. 2(a)–2(c)].

The film thickness can be estimated from the analysis of the cross-sectional images presented in Figs. 2(d)–2(f) using ImageJ software.[50] Similar estimated film thicknesses were obtained for all films thermally treated in different atmospheres, with an average value of 98.47 $\pm$ 3.09 nm. Since the conditions of the growth stage were well controlled by the microwave, similar morphologies and thicknesses were expected and confirmed by SEM analysis. In addition, by analyzing the cross-sectional images, a good interface between the conductive substrate and the hematite is observed, with a large number of rods apparently growing parallel to the substrate.

Following with the film characterization evaluating the important requirement that hematite needs to fulfill to be applied as photoanodes in PEC devices the optical properties was measured. Hematite films were analyzed using electronic absorption spectroscopy in the visible-ultraviolet region with a bare substrate used as a reference (blank). The absorbance values were normalized by the thicknesses estimated from the SEM images [Figs. 2(d)–2(f)] to obtain the absorption coefficient. Figure 3 illustrates the change in absorption coefficient as a function of wave length for all the hematite films synthesized and thermally treated under different atmospheres. This plot helps identify possible electronic transitions resulting from the use of different atmospheres during the thermal treatment in addition to the well-known and typical electronic transitions related to the optical band gap of hematite.

For all hematite films a quite similar value of maximum absorption was observed as being slightly above of 550 nm. However, the absorption profile of films thermally treated under an O_2 or N_2 atmosphere (blue and red line, Fig. 3) exhibits a different behavior compared to films prepared in air (black line, Fig. 3). The spectra depicted by the blue and red lines exhibit shoulder peaks (at around 360, 430, 530, 650, 750 nm) related to a specific electronic transition in the hematite structure. It is well known in solid state physics that the insertion of dopants and the use of an inert or oxidizing atmosphere during the annealing process can result in defects (such as vacancies). For instance, the band at around 640 nm could be attributed to an energy level between the conduction and valence bands due to the presence of a created defect, as previously reported.[51–53] Indeed, it's common the use of controlled atmosphere (Ar, O_2, N_2, etc.) during the thermal treatment for favoring the defect formation making it able to create sub levels between the valence band and conduction hematite, affecting positively or negatively the charge transfer process. However, in the present study, this change in the optical absorption spectra at 640 nm can be related to the presence of certain amount of porosity (which has different refraction index), illustrated in the top-view of SEM images, caused by using different atmospheres during the thermal treatment. This is a plausible explanation once the estimated for all hematite electrodes showed a quite similar thickness.

To understand the effect of the inert and oxidizing atmosphere during thermal treatment on the properties of the hematite film, we carried out linear voltammetry experiments under dark and illuminated conditions. The photocurrent density of all the hematite films was measured by shining light on both sides (back and front) of the film, however no difference was noted. Figure 4(a) exhibits the photocurrent density versus voltage (measured against a reversible hydrogen electrode as reference) curves of all the hematite films in the presence and absence of light. As expected, in the absence of light, the hematite films do not generate any current, as represented by the black dashed lines in Fig. 4(a).

From the curves shown in Fig. 4(a), the photocurrent density response at 1.23 V_{RHE} was around 0.09, 0.15, and 0.50 mA/cm^2 for hematite films prepared in air (black line), O_2 (blue line), and N_2 (red line), respectively. The maximum values of photocurrent for these three films at 1.6 V_{RHE} follow the same order: air (0.12 mA/cm^2),

https://doi.org/10.1557/jmr.2015.353 Published online by Cambridge University Press

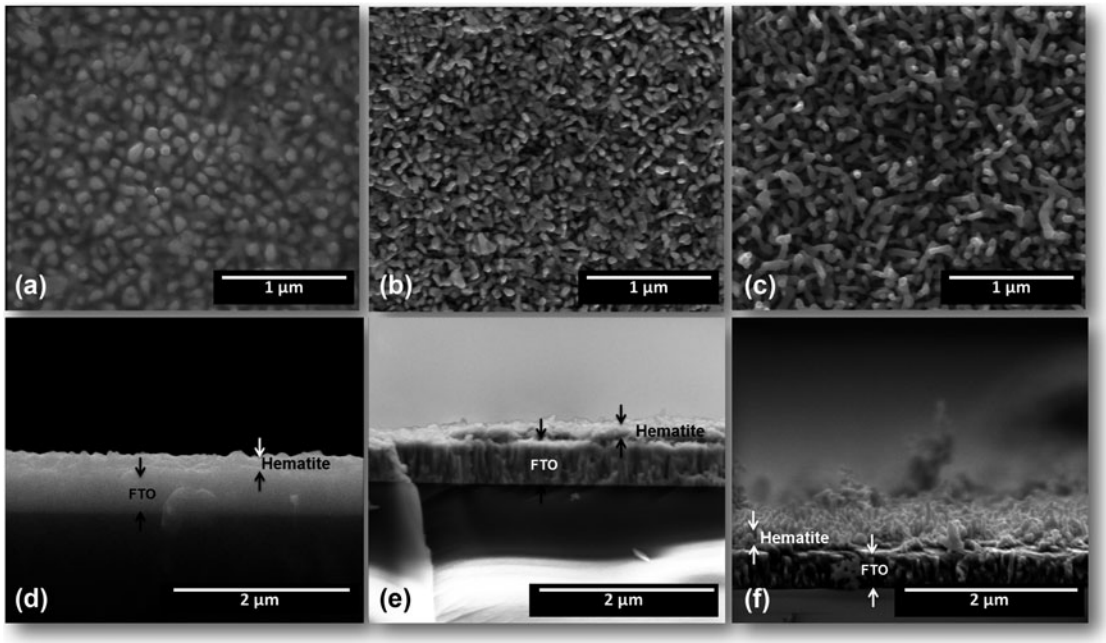


FIG. 2. Morphological characterization of the films thermally treated at 750 °C in different atmospheres by SEM observations. Top-view images of hematite thin films treated in (a) air, (b) O_2, and (c) N_2. Cross-sectional images for hematite films prepared in (d) air, (e) O_2, and (f) N_2.

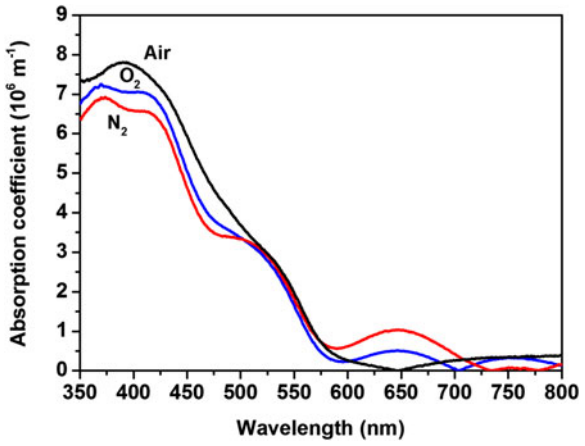


FIG. 3. Absorption coefficient as a function of wave length for a hematite film thermally treated at 750 °C for 30 min in air (black line), N_2 (red line), and O_2 (blue line). The conductive glass substrate was evaluated and used as a baseline.

O_2 (0.39 mA/cm^2), and N_2 (0.93 mA/cm^2). Additionally, the photocurrent stability at 1.23 V_{RHE} applied potential under illuminated conditions was carried out by chronoamperometry measurements. Figure 4(b) corresponds to the curves of photocurrent versus time (60 min) for all the three hematite films under illumination; the films show very good stability, which is an important requirement for their application in PEC devices. It's worth to mention that the slight difference in stability observed comparing O_2 and Air hematite with N_2 hematite electrode is consistent with the idea that samples thermally treated at rich O_2 atmosphere can have it solid–liquid interface improved, whereas the N_2 enhance the solid–solid interface. This explanation is convincing once we known that the electrochemical measurements evaluate the transference of charge in the solid–liquid interface.

Measurements of the IPCE at 1.23 V_{RHE} applied potential as a function of the wave length (nm) were also carried out for all three hematite films. IPCE values for hematite films prepared in air (black dot), O_2 (red dot), and N_2 (blue dot) were found to be around 4.5, 7.5, and 14.0% at 320 nm, and higher values of 5.6, 9.8, and 17.3% were observed at 400 nm (see Fig. S1). In general, hematite films synthesized in this study exhibit increased efficiency under an O_2 atmosphere, which increases even more under a N_2 atmosphere. Usually, the enhancement in photocurrent density under an O_2 or N_2 atmosphere can be related to increases in the charge transport, e.g., reducing the charge recombination process. The IPCE data obtained at 1.23 V_{RHE} were integrated with the data measured using a standard solar spectrum (simulated using AM 1.5 G filter adjusted at 100 mW/cm^2) showing photocurrent density calculated value similar in both measurements (difference lower than 10%), which ensure the quality of calibrated sunlight simulator used.

To evaluate the factors that contribute to the enhancement in efficiency observed for the hematite films synthesized under different atmospheres, we carried out EIS analysis in the absence of light. The electrochemical

https://doi.org/10.1557/jmr.2015.353 Published online by Cambridge University Press

impedance data were analyzed in terms of Mott–Schottky and Nyquist plots, as displayed in Fig. 5. The Mott–Schottky plot [inverse square of the capacitance (10^{10} F^{-2}) as a function of the potential applied (V_{RHE}) at a frequency of 1 kHz] was used to estimate the donor charge density (N_D) and flat band potential (V_{fb}).

The above mentioned electronic parameters were determined using Mott–Schottky plots and Eq. (3) (Ref. 54):

$$\frac{1}{C^2} = \frac{2}{e\varepsilon\varepsilon_0 N_D A^2}\left[(V - V_{fb}) - \frac{KT}{e}\right] \quad , \qquad (3)$$

where C is the capacitance, e is the elementary charge, ε_0 is the permittivity of vacuum, ε is the dielectric constant [hematite, $\varepsilon = 80$ (Ref. 42)], N_D is the donor density, A is the geometrical area, K is the Boltzmann constant, T is the temperature, V is the applied potential, and V_{fb} is the flat band potential.

From a good linear fitting ($R^2 > 0.99$ for all films) of the Mott–Schottky plots between 0.5 and 0.9 V_{RHE}, the donor charge density for the three hematite films was found to vary from 10^{-19} to 10^{-20} cm^{-3}; the maximum N_D value was observed for films thermally treated under a N_2 atmosphere. The flat band potential (V_{fb}) was measured as the value of the x-intercept of the linear fit

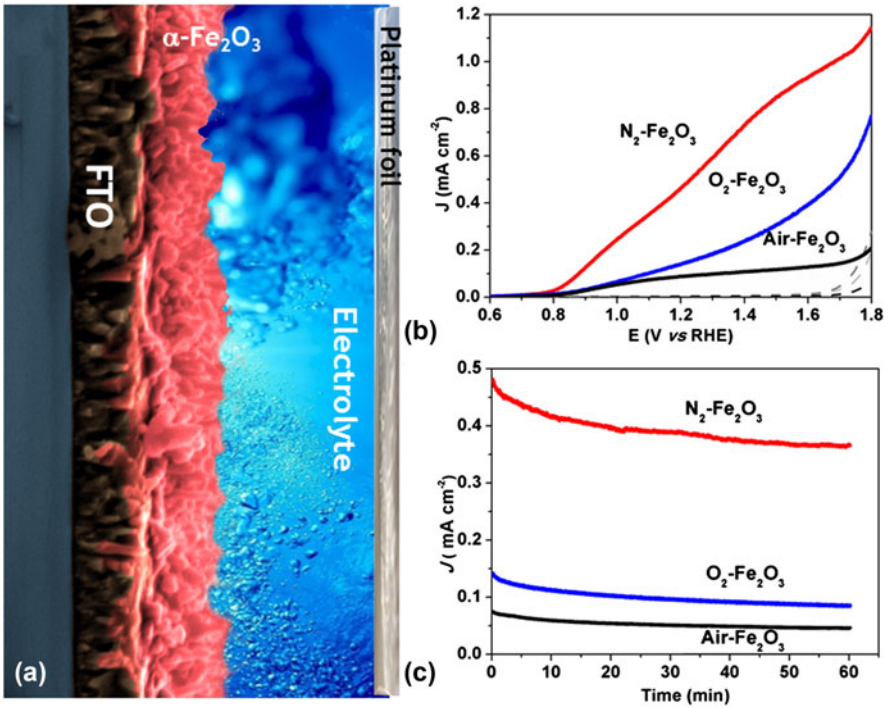


FIG. 4. Photoelectrochemical measurements performed under dark and illuminated conditions for all three hematite films synthesized; (a) schematic representation of hematite films water oxidation reaction under sunlight illumination producing O_2 gas; (b) linear sweep voltammetry in the dark (black dashed lines) and under illuminated conditions; (c) photocurrent stability at 1.23 V_{RHE} for 1 h under illumination. The illuminated conditions were simulated by sunlight simulator coupled with an AM 1.5 G filter and adjusted at 100 mW/cm^2. Electrolyte: 1 mol/L of NaOH in distilled water with the pH adjusted to 13.6.

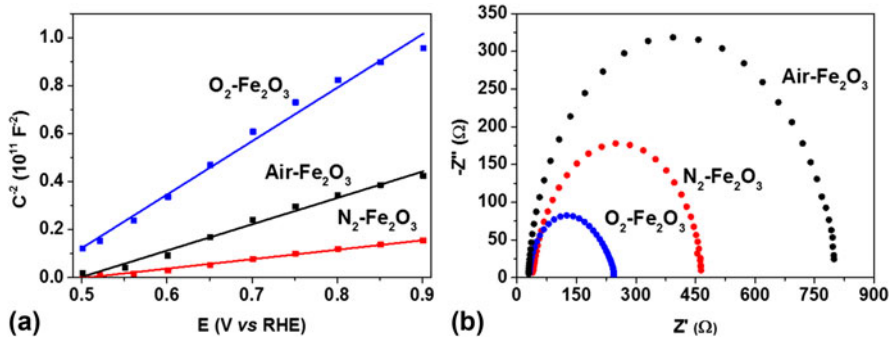


FIG. 5. EIS was conducted at room temperature in the absence of light for hematite films synthesized over 2 h with additional thermal treatment at different atmospheres and analyzed by (a) Mott–Schottky and (b) Nyquist plots. Electrolyte: 1 mol/L of NaOH in distilled water with the pH adjusted to 13.6.

https://doi.org/10.1557/jmr.2015.353 Published online by Cambridge University Press

of Mott–Schottky plot; the value was determined to be around 0.4–0.5 V_{RHE}. The N_2 atmosphere promoted a slight shift to more anodic potential of the V_{fb} of hematite films. This shift can positively affect the band bending, increasing the charge separation process and resulting in a better photoelectrochemical performance, as illustrated in Fig. 4. The value of band-bending or depletion layer width (W) was determined for all three films in triplicate using the electrochemical impedance data and Eq. (4):

$$W = (2\varepsilon\varepsilon_0(V - V_{fb})/eN_D)^{1/2} \quad , \qquad (4)$$

where V is the applied potential (at 1.23 V_{RHE}) and all the other parameters in this equation have already been defined. As aforementioned, a lower value of W was achieved for films prepared under a N_2-atmophere, suggesting that N_2 could be favoring a more efficient transfer of charge owing to an enhancement in the electric field across the W. All estimated parameters from electrochemical impedance data analyzed by the Mott–Schottky plot are summarized in Table I. In addition, the pseudo-overpotential for the water oxidation reaction at the hematite film surface was estimated using the relation ($\eta_{ox} = V_{onset} - V_{fb}$) between the onset potential (V_{onset}) under AM 1.5 G illuminated conditions and the flat band (V_{fb}) potential.[55] Compared to hematite films prepared under air and O_2 atmospheres, those prepared under a N_2 atmosphere exhibited a lower value of η_{ox} at around 0.25 V_{RHE}. Usually, for PEC applications, the ideal value of η_{ox} is zero or values close to zero so that there is no need for external excitation. Nyquist plot analysis was also done to observe the effect of different atmospheres on the resistance of charge transfer at the hematite film surface.

Figure 5(b) shows the Nyquist plot obtained in dark conditions at room temperature, and the resistance for charge transfer for O_2-hematite films was lower than those for the other two films. This result is commonly observed for O_2-treated samples. It is well known that the O_2-atmosphere improves the semiconductor surface quality favoring the solid–liquid interface for chemical reactions, but it negatively affects the solid–solid interface (FTO substrate–hematite layer interface). Once the electrochemical measurement is evaluating the transference of charge between semiconductor surface–liquid interfaces (electrolyte) the lower resistance for charge transfer obtained for O_2-hematite films is not a surprise. Although a slight increase in the donor charge density (1 order of magnitude) for hematite films synthesized under N_2 was observed. In fact, the N_2 treatment enhanced the solid–solid interface, favoring charge collection and transport, but it has a negative impact to the semiconductor–liquid interface. Moreover a better photocurrent response achieved for the N_2-hematite film cannot be explained as being a simple electronic effect caused by the inclusion of oxygen vacancies. Thus, these results motivated further investigation into the effects of the atmosphere used during the preparation of the hematite film.

To eliminate any ambiguous interpretation about the effect of the atmosphere used during thermal annealing, the photoelectrochemical measurements were carried out using a modified aqueous electrolyte by adding a controlled amount of H_2O_2 solution (0.1 mol/L). It is well known that the addition of H_2O_2, as hole scavengers, could significantly improve the water oxidation activity, showing almost ideal behavior possible for the synthetic material obtained by choose method.[55] Indeed, it is a useful strategy to diagnose possible parameters that are limiting the achievement of high performance. The photoelectrochemical performance of the hematite film prepared under hydrothermal conditions with an additional thermal treatment in air was measured in the absence [black line, Fig. 6(a)] and presence [green line, Fig. 6(a)] of hole scavengers. It clearly illustrates a shift in the onset potential to more cathodic potential (close to the V_{fb}) with a significant enhancement in photocurrent density. In fact, this result shows that photogenerated holes are available in the air-hematite film for the water oxidation reaction; however, in the absence of hole scavengers, it is likely that a very low amount of photogenerated charge is effectively used. In the case of the N_2-hematite film only a slight shift in the onset potential with low photocurrent improvement was observed on comparing the photoelectrochemical performance without [red line, Fig. 6(b)] and with [green line, Fig. 6(a)] hole scavengers. Moreover, the photocurrent profile in the presence/absence of hole scavengers is very similar at high applied potential. In addition, the photocurrent density of films prepared under N_2 was similar

TABLE I. Photo and electrochemical parameters estimated from measurements conducted at room temperature in the absence and presence of light. Photocurrent density (J) at 1.23 V_{RHE} and 1.6 V_{RHE}, donor charge density (N_D), flat band potential (V_{fb}), pseudo-overpotential (η_{ox}), and the depletion layer width (W).

	J (mA/cm^2) (1.23 V_{RHE})	J (mA/cm^2) (1.60 V_{RHE})	N_D (cm^{-3})	V_{fb} (V_{RHE})	η_{ox} (V_{RHE})	W (nm)
Air–Fe_2O_3	0.09	0.12	4.73×10^{19}	0.49	0.32	17
O_2–Fe_2O_3	0.15	0.39	1.54×10^{19}	0.41	0.36	27
N_2–Fe_2O_3	0.50	0.93	1.14×10^{20}	0.51	0.25	10

https://doi.org/10.1557/jmr.2015.353 Published online by Cambridge University Press

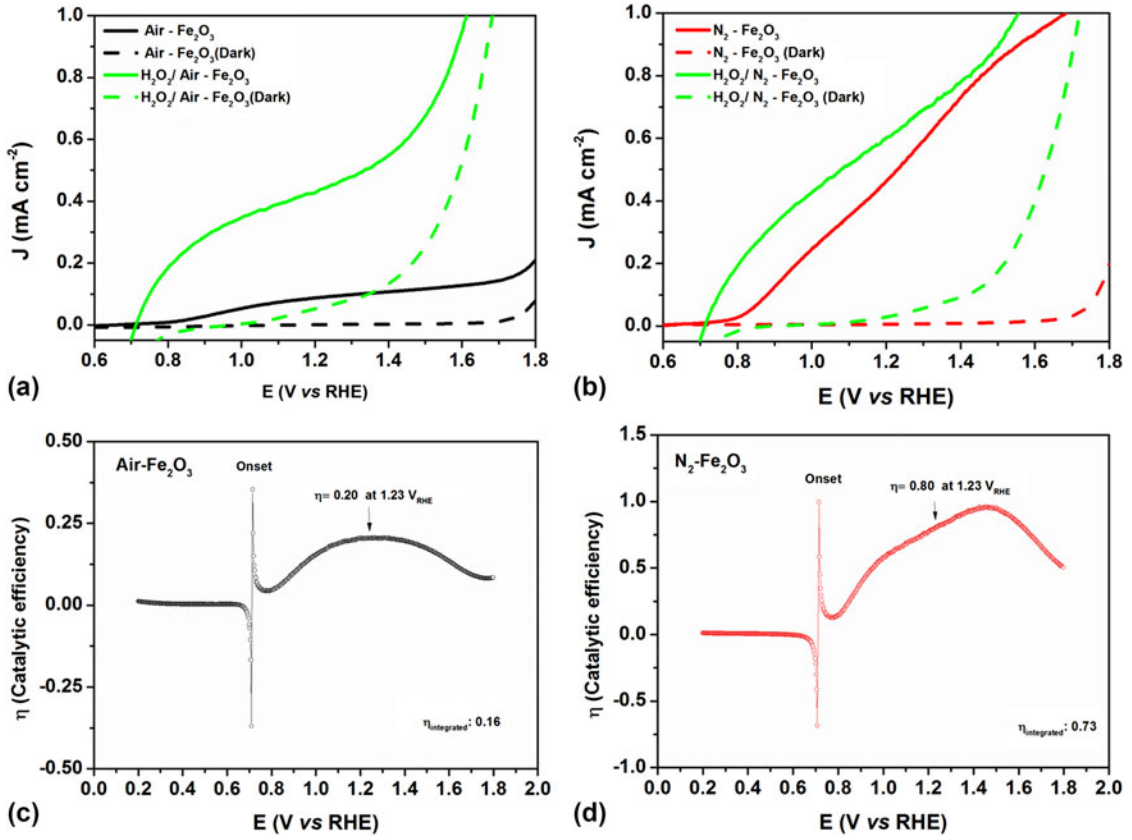


FIG. 6. Linear voltammetry sweep performed under illuminated conditions in the presence and absence of H_2O_2 added in the electrolyte solution (a) air-hematite film; (b) N_2-hematite film; catalytic efficiency, η, from the ratio between both the photocurrent response measured in (a) and (b) was estimated by (c) air-hematite film and (d) N_2-hematite film. Electrolyte: 1 mol/L of NaOH in distilled water with the pH adjusted to 13.6. For measurement with H_2O_2, a controlled amount (0.1 mol/L) was added very slowly to avoid bubble formation.

both in the presence/absence of hole scavengers. These results lead us to believe that the N_2 atmosphere used is actuating as a "hole scavenger" increasing the catalytic efficiency for the water oxidation reaction. The enhancement in the efficiency (η) of catalytic activity is better visualized by comparing values and the curve profile exhibited in Figs. 6(c) and 6(d), for both hematite films. Note that for N_2-hematite, the catalytic efficiency reached values of around 80% whereas films prepared in air reached values of 20% at 1.23 V_{RHE}, with an overall catalytic efficiency around 73 and 16%, estimated from the onset potential to 1.8 V_{RHE}, as shown in Figs. 6(c) and 6(d). Since the electronic properties were not significantly altered, the N_2 atmosphere seems to positively affect the hematite–electrolyte interface, enhancing the catalytic efficiency, which is unusual as aforementioned before. In fact, the major effect of N_2 atmosphere here can be related to the catalytic improvement, but many others effect cannot be ignored such as the presence of oxygen vacancies. For instance, the slightly increase in the number of donor density observed, which can be related to the vacancy formation, can reduce the rate of back electron recombination contributing to the overall enhancement, as well.[45]

IV. CONCLUSIONS

In summary, pure hematite thin films were successfully synthesized for the first time in a single step at low and constant temperature under hydrothermal-assisted conditions using a commercial microwave system. This wet chemical method can be used to fabricate a very well distributed iron oxide nanostructure over the glass conductive substrate. An additional thermal treatment was carried out under different atmospheres to obtain the desired phase of iron oxide and for film surface activation. A series of characterizations were carried out for evaluating the effect of the atmosphere on all synthesized films. The top-view and cross-sectional SEM images illustrate a morphology formed by rods with thickness between 98 and 100 nm for all the three hematite films. The absorption spectra showed the presence of several additional electronic transition bands compared with hematite films prepared in air. Some of these transitions could be attributed to the inclusion of defects or oxygen vacancies, as previously reported. In addition, the slight reduction observed in the optical absorption at around 650 nm comparing the O_2 and N_2-hematite with air-hematite electrode can be related to the presence of

https://doi.org/10.1557/jmr.2015.353 Published online by Cambridge University Press

apparent porosity illustrated in the SEM images, which has different refraction index. The photoelectrochemical response of hematite films thermally treated under a N_2 atmosphere was 80 and 50% more efficient than those films produced in air and an O_2 atmosphere, respectively. This enhancement in the photocurrent response for the N_2-hematite film was not attributed to the electronic changes, as pointed out in the literature. The Nyquist plot analysis revealed a lower resistance of charge transfer for hematite films prepared in O_2. However, this result is expected since it is well known that an O_2 atmosphere improves the hematite–electrolyte interface, favoring charge transport, however, it is not effective for charge transfer in a hematite-conductive substrate interface, which could be responsible for the low enhancement in overall photocurrent density. In contrast with previous reports in the literature that a N_2 atmosphere could improve the charge transport, increase charge separation yields, and decrease the resistance for charge transfer between hematite/conductive glass substrate, in this study, the predominant effect was attributed to a significant enhancement in the catalytic efficiency. This means that the N_2 atmosphere positively affected the interface between the hematite film and electrolyte, increasing the overall photocurrent response. Indeed, as illustrated by photoelectrochemical measurements in the presence of hole scavengers, the N_2-atmosphere seems to play the same role as a hole scavengers for water oxidation. Further experiments are underway in our laboratory for optimization of the synthesis protocol and a better comprehension of the effects of thermal treatment under an oxygen deficient atmosphere.

ACKNOWLEDGMENTS

We gratefully acknowledge financial support from the Brazilian agencies of FAPESP (Grants 2011/19924-2, 2013/05471-7, 2014/50516-6 and 2014/11736-0), CAPES, CNPq (Grant No. 473669/2012-9), CEM-UFABC and CDMF (Grant No. 2013/07296-2)

REFERENCES

1. M.G. Walter, E.L. Warren, J.R. McKone, S.W. Boettcher, Q. Mi, E.A. Santori, and N.S. Lewis: Solar water splitting cells. *Chem. Rev.* **110**(11), 6446 (2010).
2. T.R. Cook, D.K. Dogutan, S.Y. Reece, Y. Surendranath, T.S. Teets, and D.G. Nocera: Solar energy supply and storage for the legacy and nonlegacy worlds. *Chem. Rev.* **110**(11), 6474 (2010).
3. M.J. Katz, S.C. Riha, N.C. Jeong, A.B.F. Martinson, O.K. Farha, and J.T. Hupp: Toward solar fuels: Water splitting with sunlight and "rust"? *Coord. Chem. Rev.* **256**(21–22), 2521 (2012).
4. K. Maeda: Photocatalytic water splitting using semiconductor particles: History and recent developments. *J. Photochem. Photobiol., C* **12**(4), 237 (2011).
5. C.X. Kronawitter, L. Vayssieres, S. Shen, L. Guo, D.A. Wheeler, J.Z. Zhang, B.R. Antoun, and S.S. Mao: A perspective on solar-driven water splitting with all-oxide hetero-nanostructures. *Energy Environ. Sci.* **4**, 3889 (2011).
6. Á. Valdés, J. Brillet, M. Grätzel, H. Gudmundsdóttir, H.A. Hansen, H. Jónsson, P. Klüpfel, G-J. Kroes, F. Le Formal, I.C. Man, R.S. Martins, J.K. Nørskov, J. Rossmeisl, K. Sivula, A. Vojvodic, and M. Zäch: Solar hydrogen production with semiconductor metal oxides: New directions in experiment and theory. *Phys. Chem. Chem. Phys.* **14**, 49 (2012).
7. R.M. Navarro, M.C. Alvarez-Galvan, J.A. Villoria de la Mano, S.M. Al-Zahrani, and J.L.G. Fierro: A framework for visible-light water splitting. *Energy Environ. Sci.* **3**(12), 1865 (2010).
8. R. van de Krol, Y. Liang, and J. Schoonman: Solar hydrogen production with nanostructured metal oxides. *J. Mater. Chem.* **18** (20), 2311 (2008).
9. B.D. Alexander, P.J. Kulesza, I. Rutkowska, R. Solarska, and J. Augustynski: Metal oxide photoanodes for solar hydrogen production. *J. Mater. Chem.* **18**(20), 2298 (2008).
10. K. Shankar, J.I. Basham, N.K. Allam, O.K. Varghese, G.K. Mor, X. Feng, M. Paulose, J.A. Seabold, K-S. Choi, and C.A. Grimes: Recent advances in the Use of TiO_2 nanotube and nanowire arrays for oxidative photoelectrochemistry. *J. Phys. Chem. C* **113**(16), 6327 (2009).
11. K. Sivula, F. Le Formal, and M. Grätzel: Solar water splitting: Progress using hematite (α-Fe_2O_3) photoelectrodes. *ChemSusChem* **4**(4), 432 (2011).
12. Y. Tachibana, L. Vayssieres, and J.R. Durrant: Artificial photosynthesis for solar water-splitting. *Nat. Photonics* **6**(8), 511 (2012).
13. K.L. Hardee and A.J. Bard: Semiconductor electrodes. V. The application of chemically vapor deposited iron oxide films to photosensitized electrolysis. *J. Electrochem. Soc.* **123**, 1024 (1976).
14. K.L. Hardee and A.J. Bard: Semiconductor electrodes. X. Photoelectrochemical behavior of several polycrystalline metal oxide electrodes in aqueous solutions. *J. Electrochem. Soc.* **124**(2), 215 (1977).
15. U. Bjoerksten, J. Moser, and M. Graetzel: Photoelectrochemical studies on nanocrystalline hematite films. *Chem. Mater.* **6**(6), 858 (1994).
16. F.L. Souza, K.P. Lopes, E. Longo, and E.R. Leite: The influence of the film thickness of nanostructured α-Fe_2O_3 on water photooxidation. *Phys. Chem. Chem. Phys.* **11**, 1215 (2009).
17. F.L. Souza, K.P. Lopes, P.A.P. Nascente, and E.R. Leite: Nanostructured hematite thin films produced by spin-coating deposition solution: Application in water splitting. *Sol. Energy Mater. Sol. Cells* **93**(3), 362 (2009).
18. R.H. Gonçalves, B.H.R. Lima, and E.R. Leite: Magnetite colloidal nanocrystals: A facile pathway to prepare mesoporous hematite thin films for photoelectrochemical water splitting. *J. Am. Chem. Soc.* **133**(15), 6012 (2011).
19. K. Sivula, R. Zboril, F. Le Formal, R. Robert, A. Weidenkaff, J. Tucek, J. Frydrych, and M. Grätzel: Photoelectrochemical water splitting with mesoporous hematite prepared by a solution-based colloidal approach. *J. Am. Chem. Soc.* **132**(21), 7436 (2010).
20. J. Brillet, M. Grätzel, and K. Sivula: Decoupling feature size and functionality in solution-processed, porous hematite electrodes for solar water splitting. *Nano Lett.* **10**(10), 4155 (2010).
21. A. Kay, I. Cesar, and M. Grätzel: New benchmark for water photooxidation by nanostructured α-Fe_2O_3 films. *J. Am. Chem. Soc.* **128**(49), 15714 (2006).
22. I. Cesar, A. Kay, J.A. Gonzalez Martinez, and M. Grätzel: Translucent thin film Fe_2O_3 photoanodes for efficient water splitting by sunlight: Nanostructure-directing effect of Si-doping. *J. Am. Chem. Soc.* **128**(14), 4582 (2006).
23. T. Hisatomi, J. Brillet, M. Cornuz, F. Le Formal, N. Tetreault, K. Sivula, and M. Grätzel: A Ga_2O_3 underlayer as an isomorphic template for ultrathin hematite films toward efficient photoelectrochemical water splitting. *Faraday Discuss.* **155**, 223 (2012).

https://doi.org/10.1557/jmr.2015.353 Published online by Cambridge University Press

24. T. Hisatomi, H. Dotan, M. Stefik, K. Sivula, A. Rothschild, M. Grätzel, and N. Mathews: Enhancement in the performance of ultrathin hematite photoanode for water splitting by an oxide underlayer. *Adv. Mater.* **24**(20), 2699 (2012).
25. L. Vayssieres, N. Beermann, S.E. Lindquist, and A. Hagfeldt: Controlled aqueous chemical growth of oriented three-dimensional crystalline nanorod arrays: Application to iron(III) oxides. *Chem. Mater.* **13**(2), 233 (2001).
26. N. Beermann, L. Vayssieres, S-E. Lindquist, and A. Hagfeldt: Photoelectrochemical studies of oriented nanorod thin films of hematite. *J. Electrochem. Soc.* **147**(7), 2456 (2000).
27. L. Vayssieres, C. Sathe, S.M. Butorin, D.K. Shuh, J. Nordgren, and J. Guo: One-dimensional quantum-confinement effect in α-Fe_2O_3 ultrafine nanorod arrays. *Adv. Mater.* **17**(19), 2320 (2005).
28. R. Morrish, M. Rahman, J.M.D. MacElroy, and C.A. Wolden: Activation of hematite nanorod arrays for photoelectrochemical water splitting. *ChemSusChem* **4**(4), 474 (2011).
29. D.K. Bora, A. Braun, R. Erni, G. Fortunato, T. Graule, and E.C. Constable: Hydrothermal treatment of a hematite film leads to highly oriented faceted nanostructures with enhanced photocurrents. *Chem. Mater.* **23**(8), 2051 (2011).
30. V.A.N. de Carvalho, R.A.S. Luz, B.H. Lima, F.N. Crespilho, E.R. Leite, and F.L. Souza: Highly oriented hematite nanorods arrays for photoelectrochemical water splitting. *J. Power Sources* **205**, 525 (2012).
31. L.C. Ferraz, W.M. Carvalho, Jr., D. Criado, and F.L. Souza: Vertically oriented iron oxide films produced by hydrothermal process: Effect of thermal treatment on the physical chemical properties. *ACS Appl. Mater. Interfaces* **4**(10), 5515 (2012).
32. M. Cornuz, M. Grätzel, and S. Kevin: Preferential orientation in hematite films for solar hydrogen production via water splitting. *Chem. Vap. Deposition* **16**(10–12), 291 (2010).
33. R.H. Goncalves and E.R. Leite: The colloidal nanocrystal deposition process: An advanced method to prepare high performance hematite photoanodes for water splitting. *Energy Environ. Sci.* **7**(7), 2250 (2014).
34. S.C. Warren, K. Voïtchovsky, H. Dotan, C.M. Leroy, M. Cornuz, F. Stellacci, C. Hébert, A. Rothschild, and M. Grätzel: Identifying champion nanostructures for solar water-splitting. *Nat. Mater.* **12**, 842 (2013).
35. C.X. Kronawitter, J.R. Bakke, D.A. Wheeler, W-C. Wang, C. Chang, B.R. Antoun, J.Z. Zhang, J. Guo, S.F. Bent, S.S. Mao, and L. Vayssieres: Electron enrichment in 3d transition metal oxide hetero-nanostructures. *Nano Lett.* **11**(9), 3855 (2011).
36. L. Xi, P.D. Tran, S.Y. Chiam, P.S. Bassi, W.F. Mak, H.K. Mulmudi, S.K. Batabyal, J. Barber, J.S.C. Loo, and L.H. Wong: Co_3O_4-Decorated hematite nanorods As an effective photoanode for solar water oxidation. *J. Phys. Chem. C* **116**(26), 13884 (2012).
37. S. Shen, C.X. Kronawitter, D.A. Wheeler, P. Guo, S.A. Lindley, J. Jiang, J.Z. Zhang, L. Guo, and S.S. Mao: Physical and photoelectrochemical characterization of Ti-doped hematite photoanodes prepared by solution growth. *J. Mater. Chem. A* **1**(46), 14498 (2013).
38. A. Mao, J.K. Kim, K. Shin, D.H. Wang, P.J. Yoo, G.Y. Han, and J.H. Park: Hematite modified tungsten trioxide nanoparticle photoanode for solar water oxidation. *J. Power Sources* **210**, 32 (2012).
39. L. Steier, I. Herraiz-Cardona, S. Gimenez, F. Fabregat-Santiago, J. Bisquert, S.D. Tilley, and M. Grätzel: Understanding the role of underlayers and overlayers in thin film hematite photoanodes. *Adv. Funct. Mater.* **24**(48), 7681 (2014).
40. W.M. Carvalho, Jr. and F.L. Souza: Recent advances on solar water splitting using hematite nanorod film produced by purpose-built material methods. *J. Mater. Res.* **29**(01), 16 (2014).
41. R.H. Goncalves and E.R. Leite: Nanostructural characterization of mesoporous hematite thin film photoanode used for water splitting. *J. Mater. Res.* **29**(01), 47 (2014).
42. I. Cesar, K. Sivula, A. Kay, R. Zboril, and M. Grätzel: Influence of feature size, film thickness, and silicon doping on the performance of nanostructured hematite photoanodes for solar water splitting. *J. Phys. Chem. C* **113**(2), 772 (2008).
43. J. Gan, X. Lu, and Y. Tong: Towards highly efficient photoanodes: Boosting sunlight-driven semiconductor nanomaterials for water oxidation. *Nanoscale* **6**(13), 7142 (2014).
44. Y. Ling, G. Wang, J. Reddy, C. Wang, J.Z. Zhang, and Y. Li: The influence of oxygen content on the thermal activation of hematite nanowires. *Angew. Chem., Int. Ed.* **51**(17), 4074 (2012).
45. M. Forster, R.J. Potter, Y. Ling, Y. Yang, D.R. Klug, Y. Li, and A.J. Cowan: Oxygen deficient α-Fe_2O_3 photoelectrodes: A balance between enhanced electrical properties and trap-mediated losses. *Chem. Sci.* **6**(7), 4009 (2015).
46. A.M. Xavier, F.F. Ferreira, and F.L. Souza: Morphological and structural evolution from akaganeite to hematite of nanorods monitored by ex situ synchrotron X-ray powder diffraction. *RSC Adv.* **4**(34), 17753 (2014).
47. D.M. Cunha and F.L. Souza: Facile synthetic route for producing one-dimensional zinc oxide nanoflowers and characterization of their optical properties. *J. Alloys Compd.* **577**, 158 (2013).
48. T. Ami and M. Suzuki: MOCVD growth of (100)-oriented CeO_2 thin films on hydrogen-terminated Si(100) substrates. *Mater. Sci. Eng., B* **54**(1–2), 84 (1998).
49. S. Shen, C.X. Kronawitter, J. Jiang, S.S. Mao, and L. Guo: Surface tuning for promoted charge transfer in hematite nanorod arrays as water-splitting photoanodes. *Nano Res.* **5**(5), 327 (2012).
50. W. Rasband: *ImageJ* (Bethesda, MD: National Institutes of Health, 2015).
51. M. Anpo and M. Takeuchi: The design and development of highly reactive titanium oxide photocatalysts operating under visible light irradiation. *J. Catal.* **216**(1–2), 505 (2003).
52. X. Pan, M-Q. Yang, X. Fu, N. Zhang, and Y-J. Xu: Defective TiO_2 with oxygen vacancies: Synthesis, properties and photocatalytic applications. *Nanoscale* **5**(9), 3601 (2013).
53. R. van de Krol and M. Gratzel: *Photoelectrochemical Hydrogen Production* (New York: Springer Science, 2012).
54. T. Lopes, L. Andrade, F. Le Formal, M. Gratzel, K. Sivula, and A. Mendes: Hematite photoelectrodes for water splitting: Evaluation of the role of film thickness by impedance spectroscopy. *Phys. Chem. Chem. Phys.* **16**(31), 16515 (2014).
55. K. Sivula: Metal oxide photoelectrodes for solar fuel production, surface traps, and catalysis. *J. Phys. Chem. Lett.* **4**(10), 1624−1633 (2013).

Supplementary Material

To view supplementary material for this article, please visit http://dx.doi.org/jmr.2015.353.

https://doi.org/10.1557/jmr.2015.353 Published online by Cambridge University Press